Biogeosciences Discuss., 11, 2759–2792, 2014
www.biogeosciences-discuss.net/11/2759/2014/
doi:10.5194/bgd-11-2759-2014

Biogeosciences Discussions
Open Access

Summer upwelling at the Boknis Eck time series station (1982 to 2012) – a combined glider and wind data analysis

J. Karstensen[1], T. Liblik[1,2], J. Fischer[1], K. Bumke[1], and G. Krahmann[1]

[1]GEOMAR Helmholtz Centre for Ocean Research Kiel, Düsternbrooker Weg 20, 24105 Kiel, Germany
[2]Marine Systems Institute at Tallinn University of Technology, MSI, Akadeemia tee 15a, 12618 Tallinn, Estonia

Received: 25 January 2014 – Accepted: 29 January 2014 – Published: 18 February 2014

Correspondence to: J. Karstensen (jkarstensen@geomar.de)

Published by Copernicus Publications on behalf of the European Geosciences Union.

Abstract

Two consecutive summer upwelling events, each lasting for less than 24 h, where surveyed in high temporal and vertical resolution at the Boknis Eck time series station (BE) in the western Belt Sea (Baltic Sea) in summer 2010 with an autonomous glider. Driven only by moderate offshore winds, both events resulted in strong cooling of surface waters (up to 5 K). Only for the second event, significant irreversible changes in the vertical stratification were observed and the appearance of low oxygen waters at the bottom indicated that the upwelling had an impact on the water column as a whole. A combination of wind and seasurface temperature data revealed that summer (June to September) upwelling at BE occurs for wind directions between 190° to 260° and with hourly averaged wind speed exceeding $4\,\mathrm{m\,s^{-1}}$. For the period 1982 to 2012 BE experience about 18 days of upwelling favourable wind conditions on average. Large interannual variability exist ranging from only 7.7 days in 2006 to more than 28 days in 1985. Surface (1 m depth) and deep water (below 25 m depth) anomalies of salinity and oxygen at the BE follow extended periods of strong upwelling favourable winds. Although seasurface temperature is good indicator for the existence of summer upwelling, the upwelling intensity does not correlate with the temperature anomaly.

1 Introduction

On seasonal time scales, the strongest stratification in the marine environment is found in summer, when warm surface waters overlay colder, deeper water masses. This intense stratification minimizes the vertical fluxes and has for example a strong impact on biogeochemical processes in the near surface layer. Different processes can enhance vertical fluxes and in turn add nutrients (and other substances) from below to the surface (see Lehmann and Myrberg, 2008, for a review for the Baltic). Since the Baltic Sea is an almost enclosed sea, any wind direction will generate upwelling at some shore and significant vertical fluxes of nutrients to the euphotic zone have been

BGD
11, 2759–2792, 2014

detected (Lips et al., 2009; Lass et al., 2010; Bednorz et al., 2013). Under certain conditions, such wind-induced upwelling may be modulated by coastal trapped waves (Fennel et al., 2010). At the seasurface, summer upwelling is rather easy to detect as a cold anomaly (Lehmann and Myrberg, 2008; Lehmann et al., 2012), however, the impact of the upwelling on a reorganization of the interior stratification is more difficult to estimate and it has been shown that in particular the intensity of the wind forcing and its temporal evolution play a major role (Myrberg et al., 2010).

Here we investigate observations of summer upwelling events at the location of the Boknis Eck time series station (BE), located in the western Belt Sea (Fig. 1). The Belt Sea is the transition zone between the Baltic Sea and the North Sea. It occupies a surface area of about 17 800 km^2 and has a mean depth of 15 m (Leppäranta and Myrberg, 2009). The vertical stratification in the Belt Sea is in general determined by the seasonal stratification imprinted by surface buoyancy and momentum fluxes. The deep layers of the Belt Sea are mainly influenced by salty and relative warm and dense water supplied by the North Sea inflow (e.g. Jakobsen et al., 2010). Although specific wind/sea level situations support extensive inflow events of North Sea water (e.g. Gustafsson and A. Omstedt, 2009), limited inflow always exists through the estuarine circulation driven by the outflowing low salinity water in the upper layer. Sluggish ventilation paired with strong stratification in summer drives in many parts of the Belt Sea a depletion of oxygen in the bottom layers. However, in winter overturning of near surface waters typically re-ventilates the deep layer waters.

The BE is a time series site that been sampled by regular ship visits (approximately once a month) since 1957 and a variety of parameters with relevance for multiple disciplines (physical, chemical and biological) are routinely measured (e.g. Schweiger et al., 2007; Bange et al., 2010; Dale et al., 2011; Bertics et al., 2013; Dähnke and Thamdrup, 2013). The coarse temporal resolution and the sampling at selected standard depth, paired with short term and small scale variability, makes it difficult to detect statistically significant long term trends, at least for the BE hydrographic recording (e.g. Hoppe et al., 2013). This is particularly true for the summer months, when the water column is well stratified but not ontinuously sampled.

Given the episodic nature of upwelling and its spatial variability, high-resolution sampling in time/space is required to provide the observational database to investigate processes in shallow seas. Scanfish-type systems, which are operated from moving ships, are rather well established. Autonomously operating systems, but which require only limited human intervention and can be operated over extended periods of time are rare. Recently, moored vertical profiling systems have been demonstrated to be a useful new tool for high-resolution sampling. Liblik and Lips (2012) detected quasi-stationary stratification patterns that occur on time scales of 4 to 15 days and found to be related to atmospheric forcing. In this particular case, the vertical profiles were acquired every 3 h, covering the depth range between 2 m and 50 m depth with a vertical resolution of 10 cm.

Another emerging system for autonomous high-resolution sampling, and which was also used for this study, is an underwater glider. Gliders are autonomous vehicles that utilize vehicle buoyancy changes for vertical and horizontal movement. They are remotely controlled via satellite telephone communication. Data is accessible in near-real time, the sensor payload is flexible, and they can be optimized for surveying shallow depth waters (30 m). Although gliders have been used in many surveys in the open ocean as well as in coastal areas (e.g. Ruiz et al., 2009; Ramp et al., 2009), to our knowledge no application to the Baltic Sea has been reported so far.

This paper is structured as follows: the next section provides an overview of the data that has been used for the analysis (glider, satellite, BE, and meteorological station data). The approximately one week glider data sections of physical and biogeochemical variables are described in the following section and two upwelling events, that occurred during the survey, are analysed in more detail. Based on concurrent meteorological observations, upwelling favourable wind situations are isolated. Utilizing wind data for the period 1982 to 2012 the summer BE surveys under upwelling-favourable wind situations are identified. The connection between long term anomalies of selected variables recorded at BE and wind induced upwelling are discussed in the last section.

2 Data and methods

2.1 Glider survey

A high-resolution glider survey was done from 09 July 2010 to 16 July 2010, about 500 m north of the nominal BE position (54°31.77′ N, 010°02.36′ E). The glider was commanded to operate in a "virtual mooring mode", defined by two waypoints separated by about 750 m and located at the 20 m isobath (Fig. 1). Occasionally the glider left the virtual survey line due to short-term current events and drifted into water of different depth (up to 25 m toward the southeast and less than 10 m towards the northwest).

The deployment and recovery of the glider were conducted from the RB *Polarfuchs* of the University of Kiel, Germany. The deployment was prepared by utilizing historical BE time series data, in particular the glider was ballasted to be neutrally buoyant for a density of 1011 $kg\,m^{-3}$ and a vertical density range of 8 $kg\,m^{-3}$ was expected. The survey area is marked as a "restricted area" in the navigational charts and as such no ship traffic was expected during the operation.

The glider was a shallow depth (configured for 30 m water depth) SLOCUM electric glider. The scientific payload included a SeaBird SBE41 "temperature, conductivity, pressure" probe, a turbidity/chlorophyll *a* (fluorescence) WetLabs ECO FLNTU Puck, and an AADI oxygen optode 3830. The scientific data was recorded with a sample rate of 1 Hz (oxygen with 0.5 Hz) and approximately 700.000 (oxygen 350.000) data points of each variable were collected during the survey. On three occasions the glider ventured into shallow waters where it stranded at the sea floor. It remained there until a time-out (4 h) was triggered and the glider's autonomous system decided to change the buoyancy to let the vehicle ascend to the sea surface again.

The derivation of the salinities generally followed the procedure described by Garau et al. (2011). They had shown that applying a glider speed dependent delay to the temperature allowed for the calculation of optimal, i.e. spike free, salinities. Optimal results were, for the average glider speed of 0.52 $m s^{-1}$ (2 kn) achieved with a correction amplitude α of 0.14 and a delay time scale τ of 9.7 s. The other sensors (turbidity, fluorescence, oxygen) were not corrected and the data presented here is based on the original factory calibrations. The data is internally recorded as a time series along the flight path, while for the analysis the data was interpolated onto a regular depth grid of 0.5 m vertical resolution. As such the originally slanted profiles were considered vertical profiles. Altogether 1254 gridded downcast profiles were used in analysis. Measurements in the upper two meters are sparse due to internal vehicle control mechanisms. The data was transmitted via satellite approximately once per hour and, along with the data transmission, a GPS fix was acquired that was used by the vehicle to estimate a depth-integrated current through a dead reckoning algorithm.

2.2 BE data

The BE is located approximately 1 km from the coast at the nominal position 54°31.77′ N, 010°02.36′ E in 28 m deep water. It has been first surveyed in April 1957. Details on data collection and parameters have been described elsewhere (Bange et al., 2010; Dale et al., 2011; Bertics et al., 2013; Hoppe et al., 2013). Here we will use bottle data acquired at standard depth (1, 5, 10, 15, 20, 26/25 m). We focus on the summer months (June to September) when a significant stratification is present at the location. Our primary goal is to identify the potential impact of upwelling on individual BE surveys and as such our focus is on parameters where we expect a strong impact of the upwelling to be visible. Moreover the parameters should be accessible from BE and the glider sensor payload, namely we look at temperature, salinity, oxygen, and chlorophyll a-fluorescence.

2.3 Meteorological data

Observational data from two meteorological stations are used, Schönhagen and Kiel Lighthouse (Fig. 1). Schönhagen is a certified weather station from the National Meteorological Service (DWD, id 5930) and located approximately 12 km to the north of the BE site (Fig. 1) and close to the shore. Wind observations are acquired in 10 m height and started on 1 August 1981. Data before September 2007 was acquired at a location about 2.1 km further to the north of the current station. A somewhat shorter data set, routinely available since the 1 January 1988, stems from the Kiel Lighthouse station. The lighthouse is located on a platform erected approximately 7 km from the nearest shore, at the opening of the Kiel Fjord. Until 1992 the sensors were mounted on a mast a few 10 m away from the lighthouse and later mounted directly on to the lighthouse tower at a height of 35 m. We will also make use of the seasurface temperature (SST) data recorded at nominally 1 m water depth at the lighthouse platform.

2.4 Auxiliary data

To integrate the observations of the local glider survey into a larger spatial context, SST and chlorophyll *a* distributions derived from MODIS satellite data (McClain et al., 2004) was inspected for the period of the glider survey. Considering MODIS Terra and MODIS Aqua products, best data coverage and timing of cloud free conditions were found for the MODIS Terra images for 12 July 2010 (before upwelling) and 16 July 2010 (after upwelling).

3 Results

3.1 High resolution glider survey July 2010

The parameter distributions (Fig. 2) were constructed from glider profile data recorded approximately every 15 min. The glider operated along a zonal section of about 500 m length (Fig. 1). In the following we consider the horizontal variability along this section to be insignificant and interpret the data as being representative only for the temporal evolution of the parameter fields.

A typical summer stratification, with warm, low salinity surface water overlaying colder and more saline deeper water masses, is seen during most of the survey time (Fig. 2a and b). Two upwelling events are clearly visible in all parameter fields. The first upwelling began on early 13 July 2010 (06:00 UTC) with a peak on the same day at about 18:00 UTC when the highest surface density of 1009.5 $\mathrm{kg\,m^{-3}}$ was observed. The second event began at the early 15 July (00:00 UTC) and peaked at 18:00 UTC with an even higher surface density of 1010.7 $\mathrm{kg\,m^{-3}}$. The highest SST (observed at 0.5 m depth) was recorded in the evening of the 10 July 2010, when temperatures above 23 °C were measured. The lowest SST (below 15.1 °C) was observed at the peak of the second upwelling event (15 July 2010 18:00 UTC).

The dissolved oxygen concentrations (Fig. 2c) are highest (and close to saturation) in the surface layer and decrease rather linear with depth. Undersaturation (up to 10 %) was observed during the upwelling. Minimal concentrations of about 120 $\mathrm{\mu mol\,kg^{-1}}$ are found at the deepest sampled depth during the period of the second upwelling event. The appearance of the low oxygen waters at the bottom during the second upwelling event indicates that the upwelling had some impact on the water column as a whole.

The chlorophyll *a* fluorescence (Chl *a*) is characterized by a subsurface maximum at about 8 to 12 m depth (Fig. 2d). Concentrations are very low at the surface, except for the two upwelling events (note, the data is not corrected for any quenching effects). The turbidity distribution (Fig. 2e) resamples mostly the Chl *a* distribution, noteworthy is the increase in mixed-layer (ML) turbidity after the 12 July 2010.

The buoyancy frequency, as a measure for the vertical stability of the water (Fig. 2f), showed before the upwelling two stability maxima, one associated with the base of the ML located at about 4 to 6 m depth, and a second where the transition to the deep waters occur. The stability zone was successively uplifted and after the second upwelling event less intense. The ML was about 4 to 6 m thick, as for example can be

BGD
11, 2759–2792, 2014

seen by the homogenous oxygen concentrations. During the upwelling the ML shoaled by the uplift of isopycnals to the surface but quickly re-established with the ceasing of the wind and the relaxation of the density field.

From selected satellite maps (Fig. 3) it can be seen that the upwelling, which we observe locally with the glider, had an impact on a much larger area. A pronounced cooling is found along the coastline from Kiel Bay to Åls Island (Denmark). The upwelling front (defined by the strongest horizontal gradient in SST) was located approximately 5 to 10 km from the western coastline, i.e. the total area under the influence of upwelling was about 400 to 500 km^2.

It is interesting to note that the coldest SST observed with the glider was 3 K colder than the lowest satellite SST (Fig. 3, left), which most likely is related to the temporal sampling of the satellite. Nevertheless it demonstrates that the temporal resolution of the satellite is not optimal in determining the strength of the SST variability in the region.

Satellite derived surface Chl *a* maps (Fig. 3, right) reveal higher values in the upwelling along the coast but also reach further offshore, similar to the SST anomaly signal. The increase in Chl *a* has to be interpreted first as a result of the uplift of the subsurface Chl *a* maximum, located at about 10 m before the upwelling event (Fig. 2), and appears not to be related to enhanced productivity. As the satellite integrates over the optical depth, the glider Chl *a* concentration cannot directly be compared with the satellite concentrations.

3.2 Diagnosis of upwelling from glider data

The two upwelling events were analysed in greater detail by looking at the temporal evolution of selected parameters (Fig. 4). In particular we were interested if diapycnal (and thus irreversible) mixing was associated with the upwelling. If such short upwelling events have an irreversible impact on the interior field, these events need to be further considered e.g. in numerical modelling studies.

For the moment we will interpret the upwelling as a process that operates on a two dimensional plane. We ignore any effect diapycnal mixing may have and we further

BGD
11, 2759–2792, 2014

assume that the strength of the upwelling decreases with distance from the coast. In such a case, the coastal parallel momentum flux at the surface will force the surface water to flow offshore. In parallel, water within the density range that is successively rising to the surface will be transported onshore. The offshore transport of surface water will lead to a rising of isopycnals that goes along with an increase in potential energy (PE) of the water column. With the ceasing of the momentum input, a reversal of the circulation will set in (onshore flow in the upper layer and offshore flow below) and the original stratification should re-establish. Without any mixing, the final PE should then be similar to the initial PE.

To test whether such a simple model holds for our observations, the potential energy of the water column ($E = \rho g z_{\text{ref}}$; Simpson et al., 1990) was calculated from the in-situ density (ρ), gravity ($g = 9.81\,\text{m}\,\text{s}^{-1}$), and a reference depth (z_{ref}) chosen to be 8.5 m which is approximately the "before upwelling" depth of the highest density that outcrops during the second event.

The first event (Fig. 4, left) was forced by a steady increase in wind, starting out of a period of several days with very low wind conditions ($< 2\,\text{m}\,\text{s}^{-1}$). The maximum wind speed during the event was $7\,\text{m}\,\text{s}^{-1}$ from southwest (250°), which leads to a maximum increase in PE by about $120\,\text{J}\,\text{m}^{-3}$ ($\rho = 1009.5\,\text{kg}\,\text{m}^{-3}$ at 0.5 m depth at 17:50 UTC). With the relaxation of the upwelling favourable wind forcing, the PE reverted back and close to its initial (before upwelling) value. At most about 10 % (approx. $15\,\text{J}\,\text{m}^{-3}$) of the energy input was irreversibly transformed to a change in stratification. As such, most wind energy was invested in the lateral movement (offshore/onshore) of the water. Over the period of 18 h the density surface that resides at 6 m depth was lifted to the surface and which translates into a vertical velocity of $8\,\text{m}\,\text{day}^{-1}$ (in agreement with earlier studies e.g. Lehmann and Myrberg, 2008). Unfortunately we do not have information about the vertical structure of the flow. The only information we have is the depth-integrated flow, derived from the glider dead reckoning. This flow shows a coherent signal in relation to the upwelling event (Fig. 4e and f). With the onset of the upwelling a depth averaged (net) offshore flow is seen, this turns into a more southerly flow during the peak upwelling followed by a south-eastward offshore flow during the relaxation phase.

The second upwelling event was driven by a stronger wind forcing (Fig. 4). A preconditioning of the water column by the first upwelling event (Myrberg et al., 2010) is limited as the area was under the influence of strong easterly (100°), and as such downwelling favourable, winds (up to 10 $\mathrm{m\,s^{-1}}$). The upwelling event started with a rather abrupt (within one hour) turn of the wind to southwesterly directions (250°). The uplift of the density field lead to an increase of PE by more than 210 $\mathrm{J\,m^{-3}}$, and water from about 8 m depth was lifted to the surface (equivalent to a vertical velocity of 10 $\mathrm{m\,day^{-1}}$). After the relaxation of the density field an irreversible increase in PE by about 140 $\mathrm{J\,m^{-3}}$ ($\rho = 1000.7\,\mathrm{kg\,m^{-3}}$ at 0.5 m depth at 17:50 UTC) was found, an order of magnitude larger than during the first event. Although it cannot completely be excluded that the glider mission was terminated before the full recovery of the density field, an increase in upper layer salinity by 0.5 (not shown) suggests that significant diapycnal mixing had occurred, and water of higher density than the outcrop density must have been involved in the mixing to explain the salinity increase. The depth-integrated flow is about twice as large as for the first event. Again a net offshore flow (about 0.1 $\mathrm{m\,s^{-1}}$) during the onset of the upwelling is seen followed by a much weaker and onshore flow during the phase when the density field relaxed.

Associated with the upwelling was an increase in the surface water Chl *a* concentrations (Fig. 3). This increase can be explained, at first order, by the uplift of the subsurface Chl *a* maximum. However, along-isopycnal Chl *a* concentrations are decreasing during the upwelling (not shown here), which indicate that mixing with deeper water that has a lower Chl *a* content has taken place. In general it cannot be excluded that phytoplankton growth (and as such an increase in Chl *a*), e.g. stimulated by the entrainment of nutrient rich water into the euphotic zone, took place in parallel to the dilution, nevertheless, it was not strong enough to overcome the dilution by upwelling.

For both events it is interesting to note that the stability of the water column at the mixed layer base was enhanced during the uplift of the isopycnals (Fig. 4). The zone

Discussion Paper | Discussion Paper | Discussion Paper | Discussion Paper |

BGD

11, 2759–2792, 2014

of higher stability disappeared when it reached a depth of 2 to 3 m, which we interpret as the depth that is under the direct impact of mechanical stirring from the wind (e.g. through Langmuir Circulations).

3.3 Isolating summer upwelling events in the BE observational record

We now utilize the observations from the glider in combination with the wind and SST data to derive statistics for the summer (June to September) upwelling at the BE. Variability in the BE data is a mixture of multiple scales and processes, ranging from diurnal to decadal variability while the seasonal cycle is for many parameters the dominant one. To derive anomalies we first calculated a long-term mean seasonal cycle (Fig. 5) by grouping all BE surveys into monthly bins, considering a surface layer (standard depth 1 m) and a bottom layer (standard depth 26 m or 25 m). We consider only the BE data in the period that overlap with the time series of meteorological data from Schönhagen (1982 to 2012).

At both levels a clear seasonal signal is seen for temperature, salinity and oxygen. Maximum temperature in the upper layer is found by the end of summer (August) while in the bottom layer the maximum is shifting towards October because overturning, driven primarily by heat loss at the surface, is required for the downward propagation of warmer waters. Looking more closely, in October the temperature at both levels is rather similar which indicates that no vertical gradient exists. The deep overturn of waters in October also explains why the oxygen concentrations at depth start to rise again. Saturated surface waters are mixed into the more depleted bottom waters through the overturning process. A salinity gradient between upper and bottom layer exists year-round, with higher salinities at the deeper level. We expect that this gradient can be sustained year round by a balance of salt supply, from inflowing North Sea water at the bottom, and a net freshwater surplus at the surface, from rain/run-off.

Chlorophyll *a* shows a pronounced peak in March (spring bloom) and a second, but less developed peak in November. The variability at the spring bloom peak is large and may have to do with a subsurface Chl *a* maximum that is not adequately sampled

BGD
11, 2759–2792, 2014

by the discrete bottle samples (see also Fig. 2e), but also is a sign for pronounced interannual variability.

By subtracting the long-term monthly mean averages from individual BE summer surveys, anomalies are calculated (Fig. 6). Variability in the anomalies is large and, except in oxygen and maybe Chl *a*, robust linear trends are not detectable. From the glider data analysis we found the two upwelling events to be associated with coastal parallel to slightly off shore (210° to 260°) winds and wind speeds of at least 4 $m\,s^{-1}$ (averaged hourly). Moreover, we observed that the SST cooling during the upwelling was not found in concurrent SST data from Kiel Lighthouse station (Fig. 7, left). In turn we used any SST difference between individual BE surveys and Kiel Lighthouse larger than 2 K as an indicator for active upwelling at BE. Through this indicator we were able to improve the statistics of possible upwelling favourable conditions (Fig. 7, right) and as a consequence the directional range of upwelling favourable winds extended a bit to more offshore directions (190° to 260°).

Considering only upwelling favourable wind direction and speed combinations, the Schönhagen wind data revealed that on average about 18 days (based on cumulative sum of hours) of upwelling favourable wind situations are present at BE each summer (Fig. 8). The three years with most upwelling favourable winds include 1985 (28.7 days), 1988 (28 days), and 1998 (27.75 days) while the three years with the least upwelling favourable winds were 2006 (7.6 days), 1989 (10.2 days), and 1997 (12.5 days).

The glider survey showed that the largest SST anomalies are created even under moderate wind conditions and with only little irreversible changes in the density field (and thus, in creating anomalies through diapycnal fluxes) after the ceasing of the wind. In turn a SST anomaly at any given moment in time is only in part a good indicator for the intensity of the upwelling, while strength and persistence of the upwelling favourable winds are important control parameters. A practical measure for the time integrated impact of the wind forcing is the wind impulse (I; Haapala, 1994; Myrberg et al., 2010):

BGD
11, 2759–2792, 2014

$$I = \int_0^t c_d \rho_a U^2 \, dt \qquad (1)$$

where c_d is the drag coefficient (Large and Pond, 1981), ρ_a is the air density ($1.2\,\mathrm{kg\,m^{-3}}$) and U is the wind speed at 10 m.

BE surveys under direct upwelling influence and surveys that followed a period of strong upwelling favourable wind conditions were identified (Fig. 9 and Tables 1 and A1) by evaluation of both, the SST difference (1989 to 2012 data) and the wind impulse (1982 to 2012). We considered the mean wind impulse over 1.5 days and 3.5 days before the survey. If the 1.5 and 3.5 days values are of similar magnitude, the forcing was rather constant over time. In case the first (second) impulse is larger than the second (first) the upwelling favourable winds ceased (increased) over the 3.5 days.

4 Conclusions

High resolution glider observation recorded over 7 days in July 2010 enabled us to analyse two summer upwelling events in the western Baltic in the vicinity of the Boknis Eck Time series station (BE). The two events, characterised by different intensities of the wind forcing were observed. The direct correlation of the wind forcing with the observations of upwelling and the evidence that the upwelling affected a large area, as could be seen by satellite observations, suggests that other potential drivers of upwelling, such as Kelvin Waves along the coast (Fennel et al., 2010), did not play a significant role in the observed upwelling process.

The first upwelling was initiated by a rather continuous increase in wind to moderate speed (4 to $6\,\mathrm{m\,s^{-1}}$ from 270°). Comparing the hydrographic structure before and after the event, no significant changes were observed and as such vertical/diapycnal mixing is assumed to be small. Water from approximately 6 m depth was brought to the surface

BGD
11, 2759–2792, 2014

and a significant surface temperature drop by 5 K was observed at the peak of the upwelling. The second upwelling event was initiated by a change in wind direction, from a moderate onshore wind (10 m s^{-1}, 100°) to an offshore wind (6 m s^{-1}, 210°). The outcropping density resided at 8 m depths before the upwelling and the SST dropped by up to 5.6 K at the peak of the upwelling. Comparing the upper layer salinity before and after the upwelling and ignoring any lateral influx, water from below 10 m must have been incorporated into the upwelling. For both events depth integrated currents indicate a change in offshore/onshore flow associated with the upwelling/relaxation of the density field during/after the wind forcing.

The upwelling creates a sharp maximum in vertical stability (Fig. 4g and h) through the uplift of isopycnals, but which disappears at about 2 to 3 m depth, most likely through the mechanical stirring induced by the wind at this shallow depth range. In particular for the first event the similarity of the stratification before and after the event is remarkable and supports a two-dimensional offshore/onshore circulation scheme. A stronger forcing during the second event resulted in diapycnal mixing. It is possible that deeper layer waters, which upwelled closer to the coast (e.g. seen in the temperature gradient normal to the coast, Fig. 3), were pushed on top of the lighter water when it was advected off-shore (e.g. Reissmann et al., 2009) and the resulting overturn, enhanced by wind stirring, can result in diapycnal mixing.

At BE the most favourable wind direction for upwelling are southerly (190°) to westerly (260°) winds and with wind speeds should exceed 4 m s^{-1}. The BE site faces open waters to the north and east and as such the upwelling would follow the Ekman theory concept of coastal parallel winds for a spectrum of directions. Nevertheless, an upwelling that is forced by winds normal to the coast ("Leewirkung"; Myrberg and Andrejev, 2003) is likely to operate because of the shallow water depth. Saderne et al. (2013) also observed an upwelling event initiated by westerly winds in the Eckernförde Bay.

Inspecting hourly wind observations for the summers (June to September) from 1982 to 2012 an equivalent of 18 days of upwelling favourable wind situations per year were

BGD
11, 2759–2792, 2014

found on average. The interannual variability is large, ranging from only 7.7 days (2006) to more than 28 days (1985). Comparing the SST time series from the Kiel Lighthouse station (Fig. 10) for a year with frequent upwelling (1998; 27.8 days) with a year with less frequent upwelling (1997; 12.5 days) show much lower SST in summer for the upwelling favourable year. As Kiel Lighthouse is more than 7 km away from the coast, the local SST is not under direct control of upwelling favourable winds (see also Fig. 7, left) but more representative for the open waters. Siegel et al. (2006) have shown that summer SST in the whole Baltic Sea was one of the highest/lowest in 1997 and 1998 (within period 1990–2004), respectively. Thus it is important to bear in mind that upwelling favourable winds prevails in the BE area, when generally colder summers occur in the whole Baltic Sea region.

We inspected anomalies (relative to the long time monthly mean) in temperature, salinity, oxygen, and Chl *a* for surface (nominal 1 m depth) and deep water (standard depth 25 m/26 m) in relation to intense upwelling favourable wind situations (Fig. 6). The strongest events (Table 1), considering 1.5 as well as 3.5 days, are at very similar times and indicate that the wind impulse was not only intense but also persistent over at least 3.5 days. A prerequisite for intense upwelling (Myrberg et al., 2010). Note, the strongest SST anomalies do not resample the most intense wind impulse, and in agreement with the observations from the glider survey that showed a rather quick (order 6 h) re-stratification and significant weakening of the SST anomaly after the upwelling favourable wind forcing stopped. The wind impulse over 1.5 and 3.5 days before the peak of the two upwelling events surveyed with the glider (Table 1) indicate that the upwelling was weak. Nevertheless, the SST anomaly is the largest in the record, simply because we were able to find the peak of the upwelling. This observation confirms that the SST anomaly is not a good indicator for the intensity of upwelling, nevertheless it is a good indicator for the existence (Bednorz et al., 2013; Lehmann et al., 2012).

In the upper layer the strongest impulses are associated with colder, more saline, less oxygen, and less Chl *a* (Fig. 6) while in the deeper layer maybe warmer, more saline, higher oxygen, and no specific Chl *a* signal can be seen. For both depths the

BGD
11, 2759–2792, 2014

anomalies are consistent with upwelling of deep water (for the upper 2 m) and with inflow of surrounding deep water (below 24 m), respectively. Not all extreme events can be related to extreme upwelling and may be related to the lateral transport of anomalous e.g. my mesoscale features or related to indirect upwelling forcing e.g. by Klevin Waves.

From a technology point of view we were able to demonstrate that an autonomous glider can be navigated in the shallow Baltic Sea, which has a comparably large vertical density gradient. It can provide high temporal and spatial resolved data to support time series data interpretation. The monthly ship visits allow collecting the many other parameters, not accessible by autonomous instrumentation.

For future missions it has to be considered that this study was carried out in a restricted area and as such the glider's navigation was unaffected by ship traffic. This is only in selected areas of the Baltic Sea the case, for instance 57 000 ships pass Fehmarn Belt and another 54 000 Öresund Strait every year (HELCOM, 2010) and special attention must be given to ship avoidance strategies when surveying such areas (Merckelbach, 2013).

Acknowledgements. We thank the crew from RB *Polarfuchs* and M. Schlundt for assistance in the glider operations at sea, J. Herrford for assistance in the data preparation, H. Bange for providing the BE data and organizing the BE site. The research leading to these results have received funding from the European Union 7th Framework Programme (FP7 2007-2013), under grant agreement n. 284 321 GROOM (www.groom-fp7.eu) and by EGO-COST Action ES0904.

The service charges for this open access publication have been covered by a Research Centre of the Helmholtz Association.

References

Bange, H. W., Bergmann, K., Hansen, H. P., Kock, A., Koppe, R., Malien, F., and Ostrau, C.: Dissolved methane during hypoxic events at the Boknis Eck time series station (Eckernförde Bay, SW Baltic Sea), Biogeosciences, 7, 1279–1284, doi:10.5194/bg-7-1279-2010, 2010. 2761, 2764

Bednorz, E., Polrolniczak, M., and Czernecki, B.: Synoptic conditions governing upwelling along the Polish Baltic coast, Oceanologia, 55, 767–785, 2013. 2761, 2774

Bertics, V. J., Löscher, C. R., Salonen, I., Dale, A. W., Gier, J., Schmitz, R. A., and Treude, T.: Occurrence of benthic microbial nitrogen fixation coupled to sulfate reduction in the seasonally hypoxic Eckernförde Bay, Baltic Sea, Biogeosciences, 10, 1243–1258, doi:10.5194/bg-10-1243-2013, 2013. 2761, 2764

Dähnke, K. and Thamdrup, B.: Nitrogen isotope dynamics and fractionation during sedimentary denitrification in Boknis Eck, Baltic Sea, Biogeosciences, 10, 3079–3088, doi:10.5194/bg-10-3079-2013, 2013. 2761

Dale, A. W., Sommer, S., Bohlen, L., Treude, T., Bertics, V. J., Bange, H. W., Pfannkuche, O., Schorp, T., Mattsdotter, M. E.-K., and Wallmann, K.: Rates and regulation of nitrogen cycling in seasonally hypoxic sediments during winter (Boknis Eck, SW Baltic Sea): sensitivity to environmental variables, Estuar. Coast. Shelf S., 95, 14–28, 2011. 2761, 2764

Fennel, W., Radtke, H., Schmidt, M., and Neumann, T.: Transient upwelling in the central Baltic Sea, Cont. Shelf. Res., 30, 2015–2026, 2010. 2761, 2772

Garau, B., Ruiz, S., Zhang, W. G., Pascual, A., Heslop, E., Kerfoot, J., and Tintoré, J.: Thermal lag correction on Slocum CTD glider data, J. Atmos. Ocean. Tech., 28, 1065–1071, 2011. 2764

Gustafsson, E. and A. Omstedt, A.: Sensitivity of Baltic Sea deep water salinity and oxygen concentration to variations in physical forcing, Boreal Environ. Res., 14, 18–30, 2009.2761

Haapala, J.: Upwelling and its influence on nutrient concentration in the coastal area of the Hanko Peninsula, entrance of the Gulf of Finland, Estuar. Coast. Shelf S., 38, 507–521, 1994.2771

HELCOM: Maritime Activities in the Baltic Sea, vol. 123, 68 pp., Baltic Sea Environment Proceedings, 2010. 2775

Hoppe, H.-G., Giesenhagen, H. C., Koppe, R., Hansen, H.-P., and Gocke, K.: Impact of change in climate and policy from 1988 to 2007 on environmental and microbial variables at the time

BGD
11, 2759–2792, 2014

series station Boknis Eck, Baltic Sea, Biogeosciences, 10, 4529–4546, doi:10.5194/bg-10-4529-2013, 2013. 2761, 2764

Jakobsen, F., Hansen, I. S., Hansen, N.-E. O., and Ostrup-Rasmussen, F.: Flow resistance in the Great Belt, the biggest strait between the North Sea and the Baltic Sea, Estuar. Coast. Shelf S., 87, 325–332, 2010. 2761

Large, W. G. and Pond, S.: Open ocean momentum flux measurements in moderate to strong winds, J. Phys. Oceanogr., 11, 324–336, 1981. 2772

Lass, H.-U., Mohrholz, V., Nausch, G., and Siegel, H.: On phosphate pumping into the surface layer of the eastern Gotland Basin by upwelling, J. Marine Syst., 80, 71–89, 2010. 2761

Lehmann A. and Myrberg K.: Upwelling in the Baltic Sea – a review, J. Marine Syst., 74, S3–S12, 2008. 2760, 2761, 2768

Lehmann, A., Myrberg, K., and Höflich, K.: A statistical approach to coastal upwelling in the Baltic Sea based on the analysis of satellite data for 1990–2009, Oceanologia, 54, 369–393, 2012. 2761, 2774

Leppäranta, M. and Myrberg, K.: Physical Oceanography of the Baltic Sea, vol. 378, Springer/Praxis Publ., Berlin, Heidelberg, 2009. 2761

Liblik, T. and Lips, U.: Variability of synoptic-scale quasi-stationary thermohaline stratification patterns in the Gulf of Finland in summer 2009, Ocean Sci., 8, 603–614, doi:10.5194/os-8-603-2012, 2012. 2762

Lips, I., Lips, U., and Liblik, T.: Consequences of coastal upwelling events on physical and chemical patterns in the central Gulf of Finland (Baltic Sea), Cont. Shelf. Res., 29, 1836–1847, 2009. 2761

McClain, C. R., Feldman, G. C., and Hooker, S. B.: An overview of the SeaWiFS project and strategies for producing a climate research quality global ocean bio-optical time series, Deep-Sea Res. Pt. II, 51, 5–42, 2004. 2765

Merckelbach, L.: On the probability of underwater glider loss due to collision with a ship, J. Mar. Sci. Technol., 18, 75–86, 2013. 2775

Myrberg, K. and Andrejev, O.: Main upwelling regions in the Baltic Sea – a statistical analysis based on three-dimensional modelling, Boreal Environ. Res., 8, 97–112, 2003. 2773

Myrberg, K., Andrejev, O., and Lehmann, A.: Dynamic features of successive upwelling events in the Baltic Sea – a numerical case study, Oceanologia, 52, 77–99, 2010. 2761, 2769, 2771, 2774

BGD
11, 2759–2792, 2014

Summer upwelling in the western Baltic Sea

J. Karstensen et al.

Ramp, S. R., Davis, R. E., Leonard, N. E., Shulman, I., Chao, Y., Robinson, A. R., Marsden, J., Lermusiaux, P. F. J., Fratantoni, D. M., Paduan, J. D., Chavez, F. P., Bahr, F. L., Liang, S., Leslie, W., and Li, Z.: Preparing to predict: the Second Autonomous Ocean Sampling Network (AOSN-II) experiment in the Monterey Bay, Deep-Sea Res. Pt. II, 56, 68–86, 2009. 2762

Reissmann, J., Burchard, H., Feistel, R., Hagen, E., Lass, H. U., Mohrholz, V., Nausch, G., Umlauf, L., and Wieczorek, G.: Vertical mixing in the Baltic Sea and consequences for eutrophication – a review, Prog. Oceanogr., 82, 47–80, 2009. 2773

Ruiz, S., Pascual, A., Garau, B., Pujol, I. and Tintoré, J.: Vertical motion in the upper ocean from glider and altimetry data, Geophys. Res. Lett., 36, L14607, doi:10.1029/2009GL038569, 2009. 2762

Saderne, V., Fietzek, P., and Herman, P. M. J.: Extreme variations of pCO_2 and pH in a macrophyte meadow in the Baltic Sea in summer: evidence of the effect of photosynthesis and local upwelling, PloS One, 8, e62689, doi:10.1371/journal.pone.0062689, 2013. 2773

Schweiger, B., Hansen, H. P., and Bange, H. W.: A time series of hydroxylamine (NH_2OH) in the southwestern Baltic Sea, Geophys. Res. Lett., 34, L24608, doi:10.1029/2007gl031086, 2007, 2761

Siegel, H., Gerth, M., and Tschersich, G.: Sea surface temperature development of the Baltic Sea in the period 1990–2004, Oceanologia, 48, 119–131, 2006. 2774

Simpson, J., Brown, J., Matthews, J., and Allen, G.: Tidal straining, density currents, and stirring in the control of estuarine stratification, Estuaries, 13, 125–132, 1990. 2768

BGD

11, 2759–2792, 2014

Summer upwelling in the western Baltic Sea

J. Karstensen et al.

Table 1. Twenty most significant summer (June to September) upwelling events in relation to BE surveys (1982–2012) ordered by impulse per day (over a period of 1.5 days before the BE survey). The temperature difference between Kiel lighthouse and the BE survey as well as the wind impulse per day based on the 3.5 days before the BE survey and estimate from Schönhagen wind data are given. Top five events in each category are weighted bold. For reference the intensity as been calculated for the glider survey is given at the end of the table.

Date	Intensity (1.5 days) [$kg\,m^{-1}\,s^{-1}\,day^{-1}$]	SST difference [K]	Intensity (3.5 days) [$kg\,m^{-1}\,s^{-1}\,day^{-1}$]
21 Aug 1990	**10 475**	−2.50	**13 692**
18 Jun 1987	**10 318**	−0.15	**13 811**
15 Jul 1998	**7161**	**−4.64**	**13 122**
13 Sep 2004	**7069**	−2.58	**10 040**
11 Aug 2005	**6021**	−0.54	8059
03 Sep 1992	5750	−2.40	8809
13 Jul 2004	5250	−0.29	**10 674**
08 Sep 1997	5073	−0.95	7888
13 Jul 1989	4760	−1.86	7994
11 Jul 1996	4634	0.25	5203
15 Jul 1999	4610	−0.30	6121
27 Aug 1992	4524	−1.46	6967
06 Aug 1992	4231	**−3.40**	7718
21 Sep 2011	4186	**−2.69**	7335
09 Aug 2001	3720	**−5.06**	4793
12 Jul 2007	3708	NaN	5285
09 Jul 2008	3664	**−4.17**	5608
28 Jun 2000	3444	NaN	4518
22 Jul 1998	3183	−1.51	4947
21 Jun 2011	3126	−2.14	4904
Glider			
13 Jul 2010	1632	−5	838
15 Jul 2010	2457	−6	1679

BGD
11, 2759–2792, 2014

Summer upwelling in the western Baltic Sea

J. Karstensen et al.

Table A1. 1.5 and 3.5 days average wind impulse per day and temperature difference between Kiel lighthouse for all BE summer (June to September) surveys between 1982 and 2012.

Date	Intensity (1.5 days) $[kg\,m^{-1}\,s^{-1}\,day^{-1}]$	SST difference [K]	Intensity (3.5 days) $[kg\,m^{-1}\,s^{-1}\,day^{-1}]$
21 Aug 1990	10 475	−2.50	13 692
18 Jun 1987	10 318	−0.15	13 811
15 Jul 1998	7161	−4.64	13 122
13 Sep 2004	7069	−2.58	10 040
11 Aug 2005	6021	−0.54	8059
03 Sep 1992	5750	−2.40	8809
13 Jul 2004	5250	−0.29	10 674
08 Sep 1997	5073	−0.95	7888
13 Jul 1989	4760	−1.86	7994
11 Jul 1996	4634	0.25	5203
15 Jul 1999	4610	−0.30	6121
27 Aug 1992	4524	−1.46	6967
06 Aug 1992	4231	−3.40	7718
21 Sep 2011	4186	−2.69	7335
09 Aug 2001	3720	−5.06	4793
12 Jul 2007	3708	NaN	5285
09 Jul 2008	3664	−4.17	5608
28 Jun 2000	3444	NaN	4518
22 Jul 1998	3183	−1.51	4947
21 Jun 2011	3126	−2.14	4904
11 Jul 2001	3014	−3.05	5844
14 Sep 2005	2958	0.45	3121
12 Sep 1996	2917	−0.11	3633
12 Aug 1985	2877	NaN	4110
09 Jun 1986	2834	NaN	4394
21 Sep 2010	2763	−0.85	6670
16 Sep 1998	2713	0.06	4190
16 Jul 1985	2612	NaN	4075
10 Jun 1998	2563	0.10	6079
25 Sep 1985	2553	NaN	3139
16 Aug 2007	2468	−2.75	3267
17 Aug 1992	2435	−2.44	3577
25 Jul 2011	2422	−2.01	8055
09 Sep 1992	2312	−0.41	3399
08 Jun 1995	2295	−2.10	2817
24 Jun 2008	2283	−2.32	4907
16 Sep 1987	2254	0.00	7023
19 Aug 2008	2218	−2.01	2782
15 Sep 1986	2211	NaN	2653
21 Jun 2006	2167	−0.25	3020
18 Sep 1997	2134	−0.71	5971
02 Aug 1996	2076	−1.08	3984
12 Aug 1982	2021	NaN	3614
23 Aug 1993	1838	NaN	4070
13 Jul 1993	1831	NaN	3114
19 Aug 1998	1742	−0.09	4357

BGD
11, 2759–2792, 2014

Table A1. Continued.

Date	Intensity (1.5 days) $[\mathrm{kg\,m^{-1}\,s^{-1}\,day^{-1}}]$	SST difference [K]	Intensity (3.5 days) $[\mathrm{kg\,m^{-1}\,s^{-1}\,day^{-1}}]$
17 Jun 1991	1646	−0.56	5029
21 Jul 1988	1634	−0.97	4938
26 Aug 1998	1621	−0.00	3198
10 Sep 1991	1610	0.01	2667
14 Jun 2007	1603	0.56	3459
24 Aug 1982	1596	NaN	3149
05 Jun 1996	1493	−0.16	2206
14 Aug 1991	1429	0.10	3418
17 Aug 1999	1370	−0.00	3845
08 Jul 1998	1316	−0.26	4363
27 Jun 1996	1312	−0.28	3018
20 Jun 1988	1170	−0.08	1426
22 Aug 1988	1123	−3.74	2938
21 Jun 1994	1095	0.29	5753
27 Jul 1994	1071	−0.83	1410
24 Sep 1992	1070	−0.12	1119
05 Jun 1997	965	−0.89	1719
04 Jul 1996	937	−0.91	3679
14 Sep 1988	927	−0.42	2800
21 Jul 1986	888	NaN	2091
30 Jul 1997	856	−0.12	4668
13 Sep 1995	821	−0.29	1766
14 Jul 2009	751	−2.28	2251
14 Jun 1993	731	NaN	1306
12 Jul 2000	719	NaN	1104
25 Jul 1996	634	−0.56	1004
28 Jun 2001	587	0.18	588
18 Jun 1997	585	0.06	2637
18 Sep 1990	554	0.01	771
13 Jul 1995	523	0.67	523
02 Jul 1997	512	−0.05	1154
18 Jun 2002	500	−0.78	3593
18 Sep 1994	492	−0.28	6486
05 Jun 1985	490	NaN	541
02 Jul 1998	470	−0.03	1405
17 Sep 1999	437	NaN	517
10 Aug 2010	429	−1.33	628
17 Sep 2002	413	NaN	813
29 Jul 1998	408	0.10	499
16 Jun 1992	407	0.98	1726
17 Aug 1994	337	−0.19	3031
27 Aug 1989	289	−0.30	969
07 Aug 1986	288	NaN	3146
01 Aug 2011	288	−0.91	370
28 Jul 2005	275	−0.27	1498
08 Aug 1996	257	NaN	294
22 Jul 1991	227	−0.36	992
10 Sep 2001	175	−0.04	1617

BGD
11, 2759–2792, 2014

Table A1. Continued.

Date	Intensity (1.5 days) $[kg\,m^{-1}\,s^{-1}\,day^{-1}]$	SST difference [K]	Intensity (3.5 days) $[kg\,m^{-1}\,s^{-1}\,day^{-1}]$
17 Jun 2003	175	−0.29	1110
17 Sep 1992	162	−0.28	3580
09 Jul 2002	158	NaN	999
01 Sep 1997	157	−0.22	902
19 Jun 1990	148	NaN	2449
25 Aug 1997	146	0.55	523
17 Jun 1999	132	−0.52	137
01 Jul 2010	114	−0.59	228
27 Sep 2000	100	NaN	118
26 Sep 1996	96	−0.12	96
21 Jun 2005	81	−0.25	81
25 Sep 1997	59	0.32	658
23 Aug 1995	52	−0.18	52
15 Aug 1996	36	NaN	46
25 Jun 1998	31	−0.14	1862
20 Aug 2009	31	−1.24	811
18 Jul 1996	22	−0.01	133
13 Aug 2003	21	0.29	44
08 Sep 2003	9	0.08	25
23 Jun 2009	6	−0.71	360
11 Aug 1998	1	−0.14	886
28 Aug 1983	0	NaN	66
13 Jun 1989	0	−0.55	36
12 Sep 1989	0	−0.11	0
19 Jul 1990	0	0.08	142
16 Sep 1993	0	NaN	0
21 Aug 1996	0	1.50	0
29 Aug 1996	0	0.17	174
19 Sep 1996	0	−0.10	0
09 Jul 1997	0	0.21	0
15 Jul 1997	0	NaN	84
23 Jul 1997	0	0.09	0
05 Aug 1997	0	0.24	66
12 Aug 1997	0	−1.69	0
18 Aug 1997	0	NaN	136
01 Sep 1998	0	0.64	50
08 Sep 1998	0	0.10	0
21 Sep 1998	0	0.08	390
20 Aug 2002	0	NaN	0
15 Jul 2003	0	−1.23	505
10 Aug 2004	0	0.74	0
27 Jul 2006	0	−0.45	4
12 Sep 2007	0	−0.79	0
15 Sep 2008	0	−1.29	0
16 Sep 2008	0	−1.47	0
17 Sep 2008	0	−1.15	0
18 Sep 2008	0	−1.21	0
15 Sep 2009	0	−1.01	0
02 Jun 2010	0	−0.47	0

BGD
11, 2759–2792, 2014

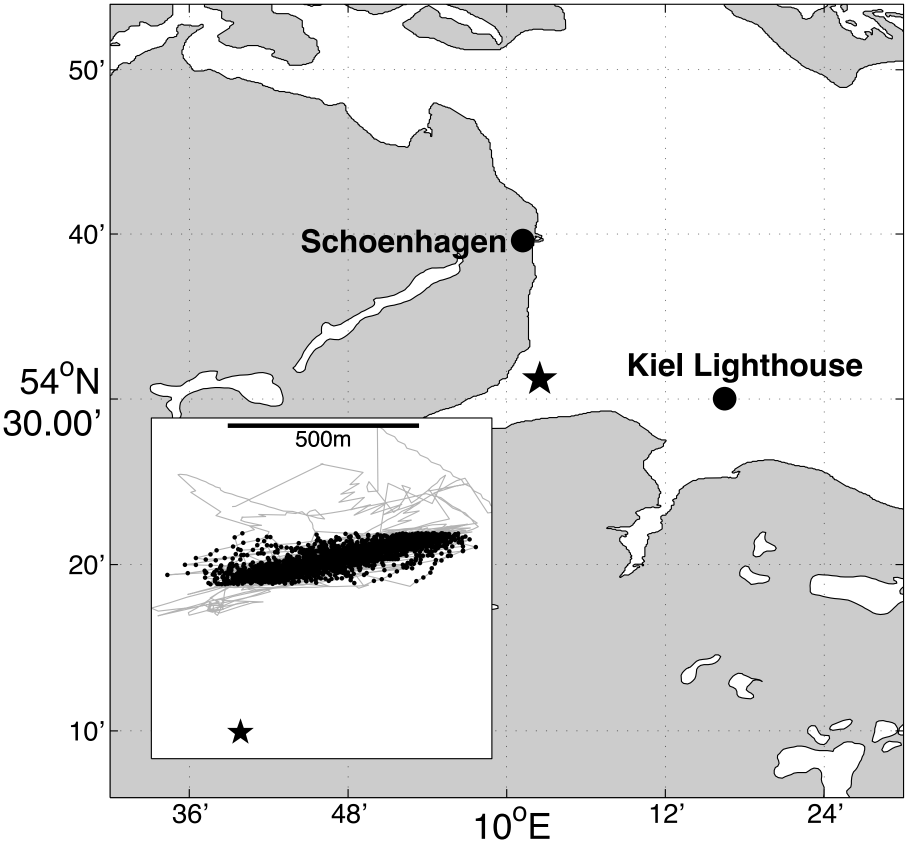

Fig. 1. Overview map with Boknis Eck time series station (black star) and the Meteorological station Schönhagen and Kiel Lighthouse. All glider tracks (grey lines) and the positions of glider observations used in this study (black dots) are shown in the inlay.

BGD
11, 2759–2792, 2014

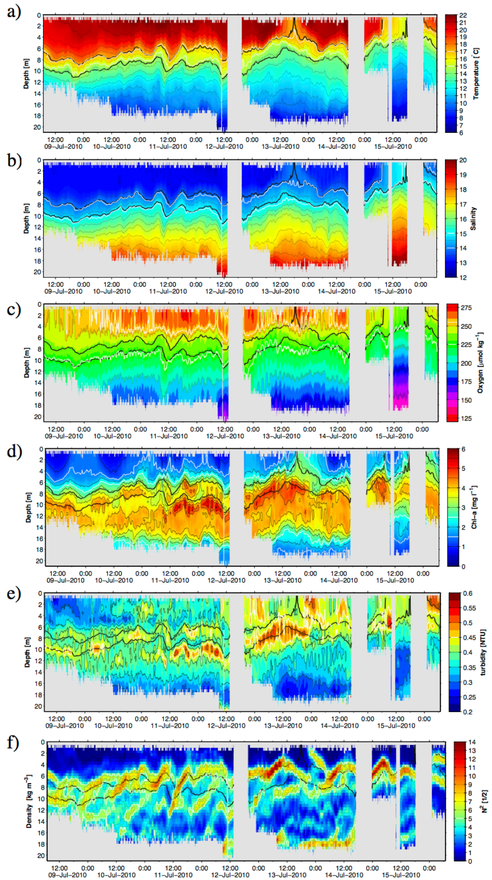

Fig. 2. **(a)** Temperature, **(b)** salinity, **(c)** oxygen, **(d)** chlorophyll *a*/fluorescence, **(e)** turbidity, and **(f)** buoyancy frequency from the glider survey. The grey areas indicate no data recordings. The white contours show selected parameters isolines (see individual colorbar). The two outcrop densities 1009.5 and 1010.7 $kg\,m^{-3}$ are indicted by black lines.

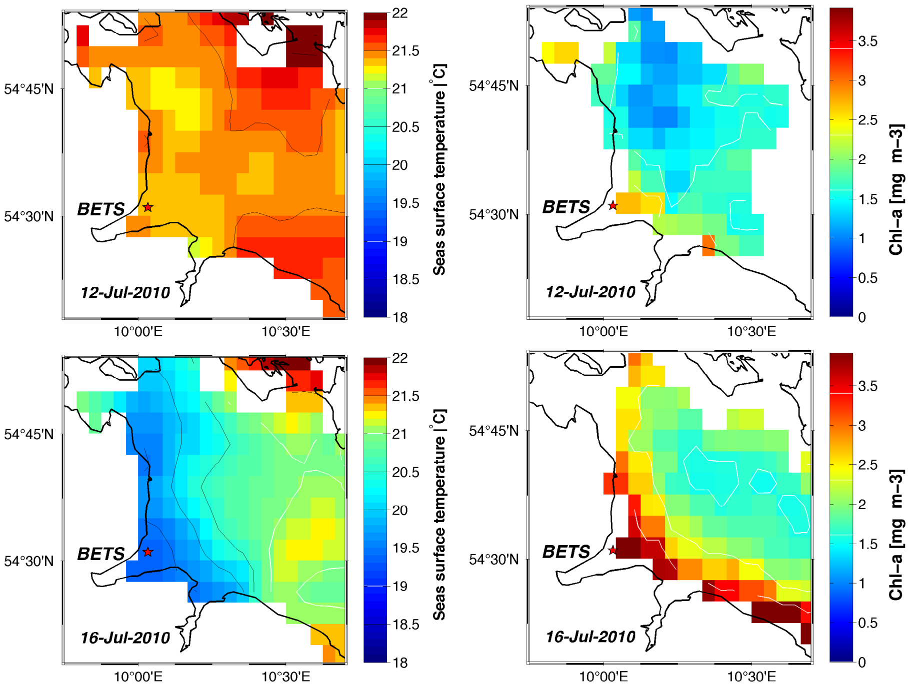

Fig. 3. Sea surface temperature (left) and chlorophyll *a* (right) distribution from MODIS satellite before the two upwelling events (upper) and after the second upwelling (lower).

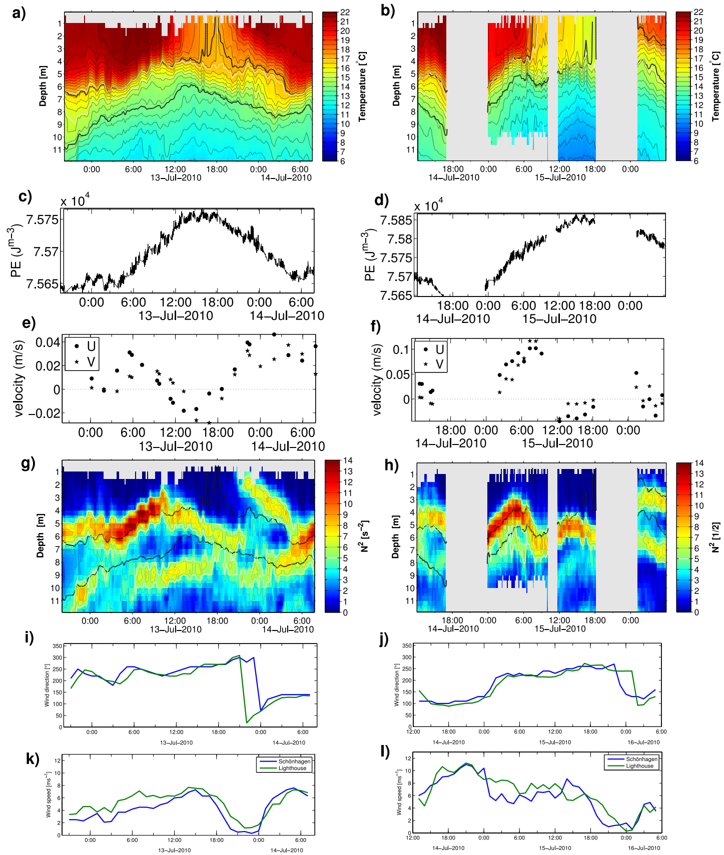

Fig. 4. Temporal evolution of selected parameters during the first (left) and second (right) upwelling event: temperature distribution in the upper 12 m **(a, b)**, potential energy of the upper 10 m **(c, d)**, vertical integrated velocity from glider **(e, f)**, buoyancy frequency **(g, h)**, wind direction at both meteorological stations **(i, j)** and wind speed **(k, l)**.

BGD
11, 2759–2792, 2014

Summer upwelling in the western Baltic Sea

J. Karstensen et al.

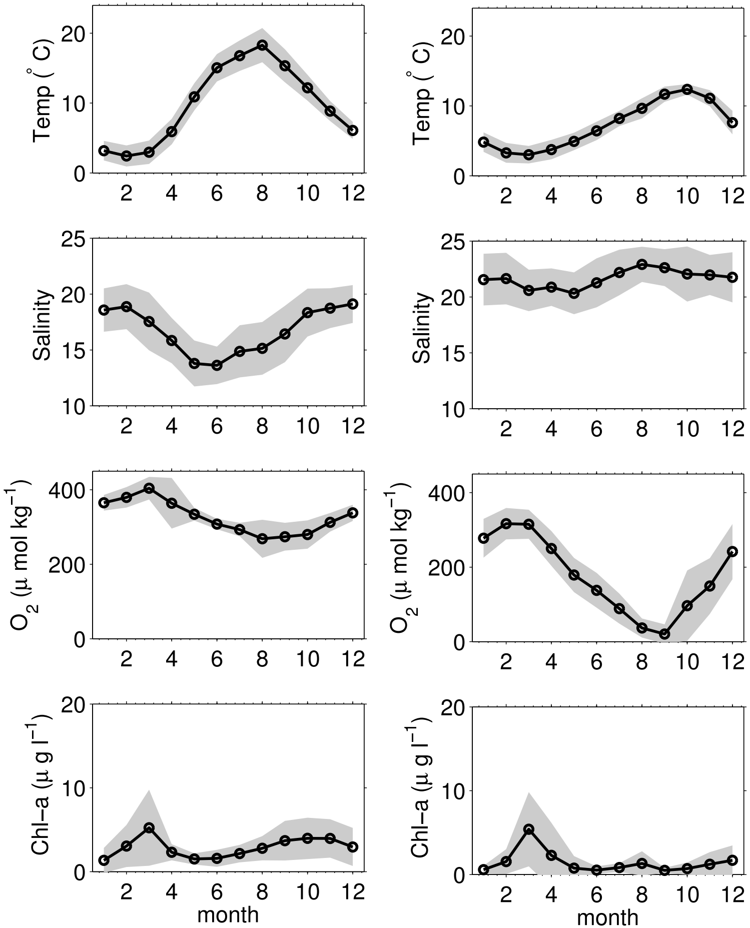

Fig. 5. Long term mean (1988 to 2012) seasonal cycle of BE parameters for all data above 2 m (left) and below 24 m (right). Grey shading indicate the standard deviation.

BGD
11, 2759–2792, 2014

Summer upwelling in the western Baltic Sea

J. Karstensen et al.

Title Page
Abstract Introduction
Conclusions References
Tables Figures
◀I ▶I
◀ ▶
Back Close
Full Screen / Esc
Printer-friendly Version
Interactive Discussion

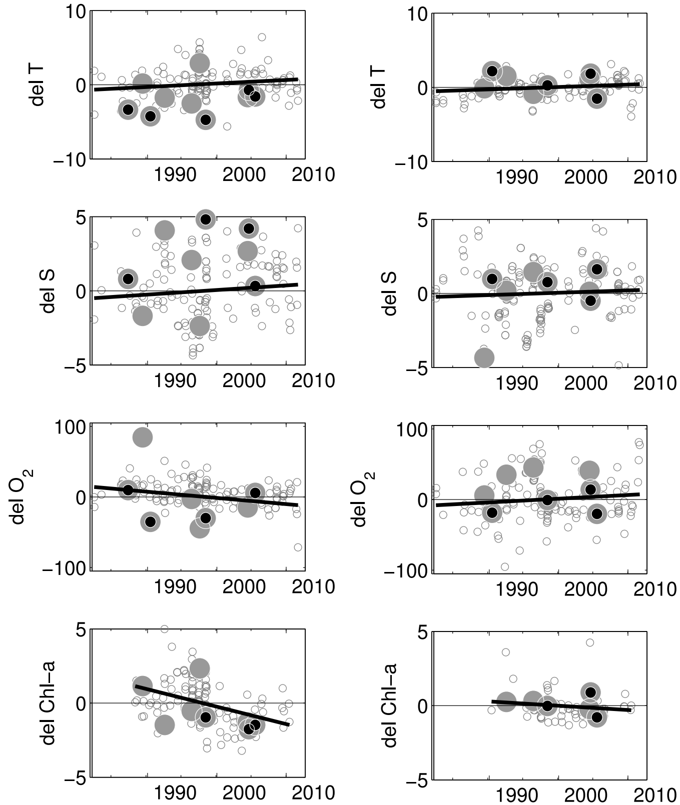

Fig. 6. Summer (June to September) anomalies (relative to long term monthly mean, see Fig. 5) of single BE surveys between 1988 and 2012. (Left) averaging all data above 2 m and (right) averaging data below 24 m (right). The black line is the linear regression to the data. Grey (black) dots indicate the anomalies that are associated with the 10 (5) strongest 1.5 days wind impulses (see Table 1).

BGD

11, 2759–2792, 2014

Summer upwelling in the western Baltic Sea

J. Karstensen et al.

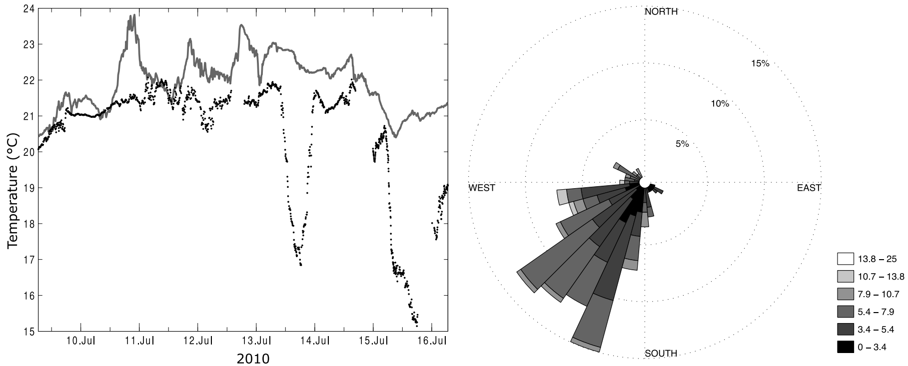

Fig. 7. (left) Seasurface temperature (at nominal 1 m depth) recorded at the lighthouse (grey line) and glider temperature (black dots) (observation closest to the surface at typically 0.5 to 1 m depth). (right) Wind rose plot of Schönhagen wind taking into account all data within 12 h before an SST difference between Kiel lighthouse and BE survey of larger 2 K was detected (considering the period 1988 to 2012).

BGD
11, 2759–2792, 2014
Summer upwelling in the western Baltic Sea
J. Karstensen et al.

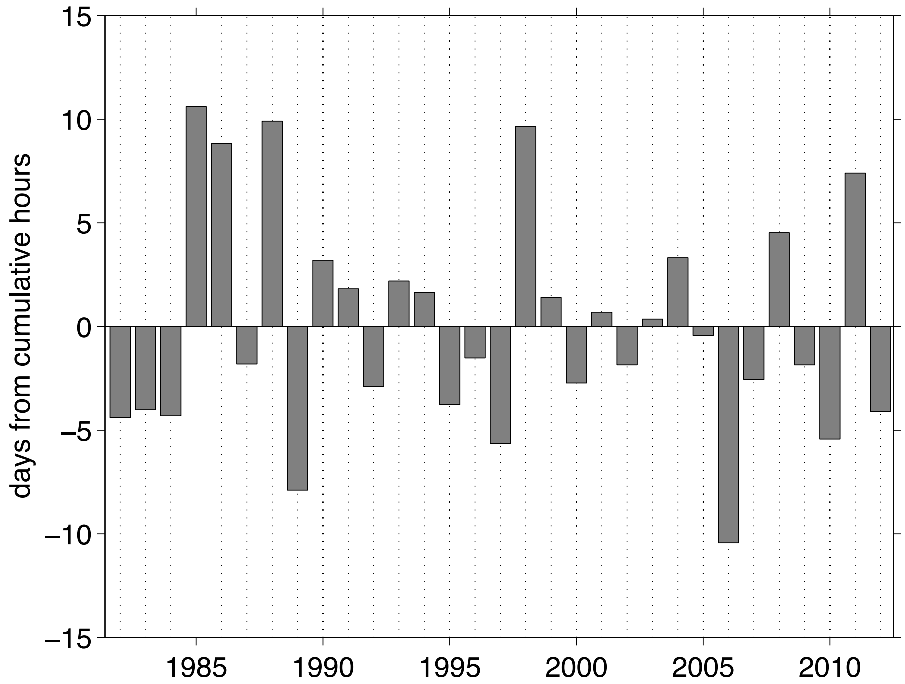

Fig. 8. Anomalous days (from cumulative sum of hours) of upwelling favourable winds (see text for definition) per year from summer (June to September) hourly observations recorded at Schönhagen station 1982 to 2012 (compare Fig. 1). Mean is 18.1 days.

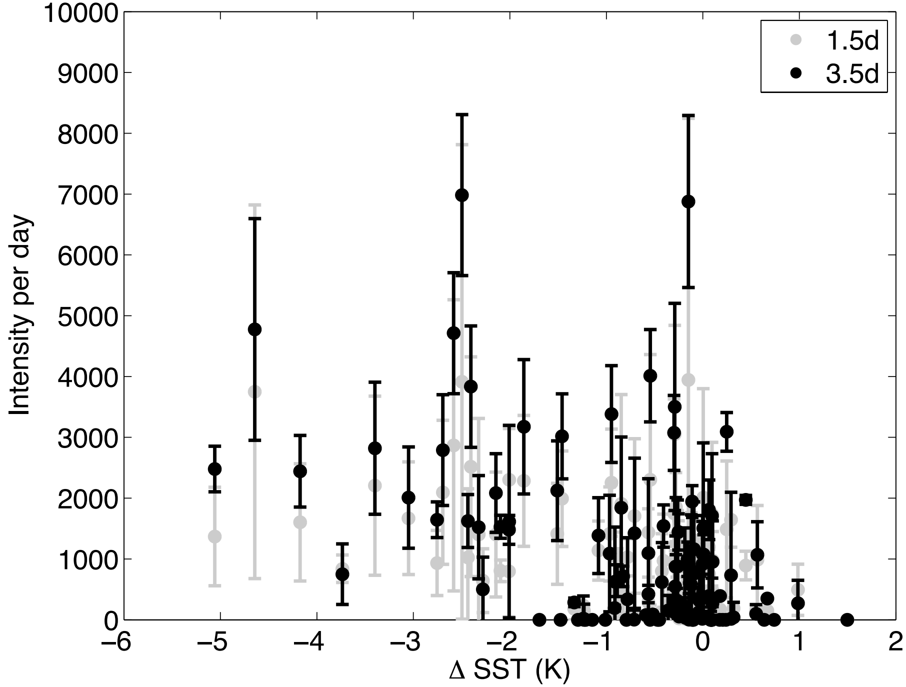

Fig. 9. Wind intensity (in $kg\,m^{-1}\,s^{-1}\,day^{-1}$) per day over the 1.5 and 3.5 days before the BE survey vs. SST difference between BE and Kiel lighthouse for the BE surveys between 1989 and 2012 (compare also Table A1). The standard deviation in wind impulse is indicated by the errorbars (see table one for details on most extreme events). Note that events without SST anomaly are not shown in this figure but in Table 1.

BGD
11, 2759–2792, 2014

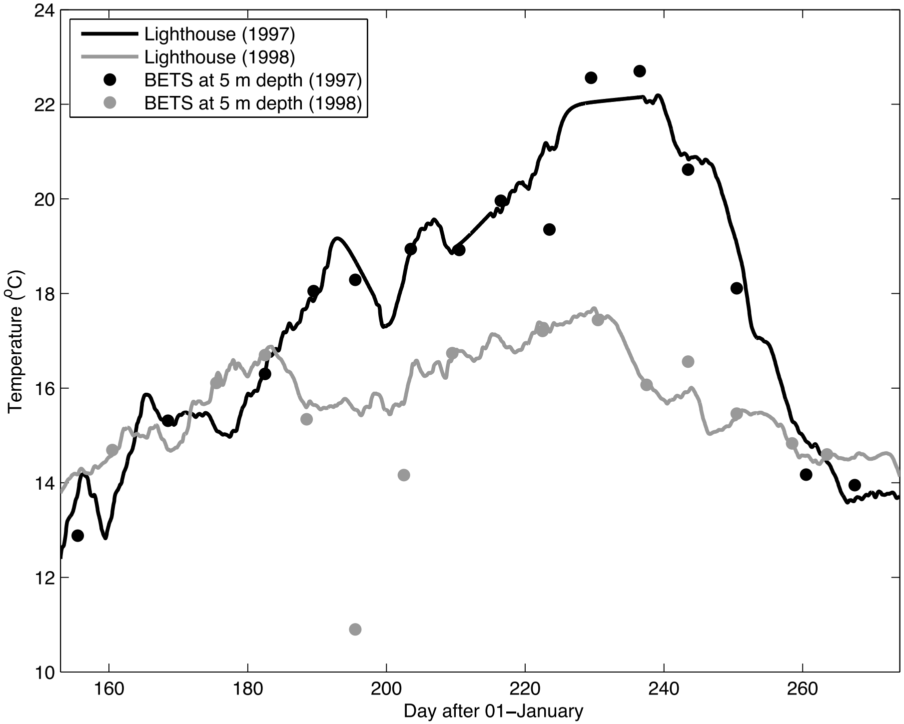

Fig. 10. Near surface temperature time series (01 June to 30 September) from Kiel Lighthouse for a selected year with high (1998) and with low frequent upwelling (1997) wind conditions. Dots indicate the respective BE temperature record (15 surveys in 1998, 14 surveys in 1997).

BGD
11, 2759–2792, 2014

Summer upwelling in the western Baltic Sea

J. Karstensen et al.